An Investigation of the Positive Column of a Hollow Cathode Arc in a Magnetic Field. Part I

F. Boeschoten *, R. Komen, and A. F. C. Sens

Department of Electrical Engineering, Eindhoven University of Technology

Z. Naturforsch. **34a**, 1009–1021 (1979); received June 28, 1979 **

The positive column of the hollow cathode arc consists of a highly ionized ($> 90\%$) and -magnetized ($\omega_{ci}\,\tau_{i,i} > 1$) plasma. In order to obtain as much as possible information about this plasma its parameters were measured as functions of radius, r, and axial distance, z. They were varied by changing the discharge parameters — arc current I, gas feed Q, magnetic field strength B, arc length L and core diameter d. Generally the discharge was fed with Argon, but Neon, Helium, Nitrogen and Hydrogen were also used.

- The radial plasma density distribution, $n_e(r)$, is approximately Gaussian for $0 \leqq r < 4$ cm ($n_e(0) \cong 2 \times 10^{14}$ part./cm^3); in axial direction the plasma density does not vary much.
- The ion temperature, T_i, is constant with radius, contrary to the electron temperature, T_e, which drops sharply near the core of the arc. In axial direction T_i drops by a factor ten from the cathode to the anode ($T_i \cong 1-30$ eV). T_i ($z = 0$) increases with arc length L.
- The whole plasma moves in axial direction from the cathode towards the anode ($v_z \cong 6 \times 10^4$ cm/s); the angular mass velocity ($\Omega \cong$ some 10^5 rad/s) is strongly sheared and decreases with temperature.
- The axial electrical field is small (0.1 to 0.2 V/cm) corresponding to a normal electrical conductivity. The radial electrical field points inwardly and varies strongly with radius ($0 \geqq E_r \gtrsim -10$ V/cm).
- Strong (nonlinear) low frequency oscillations ($\nu \cong 15$ kHz) are generated spontaneously in the plasma; these oscillations are due to the Kelvin-Helmholtz instability.

As is shown in Part II of this investigation, the observed behaviour of the plasma column may be satisfactorily explained by the two fluid model with MHD ordering. Due to viscous effects (i, i collisions) the sheared plasma rotation has big consequences for the transport of particles and energy.

1. Introduction

With a hollow cathode arc is meant here a low pressure arc which is sustained in a vacuum environment in the presence of a strong magnetic field; gas is fed through a hot glowing cathode tube (about 2200 °C) into the vacuum chamber. Simply stated, the gas is very effectively ionized and heated in the cathode region and the created plasma streams from there along the magnetic field towards the anode where a large part of it recombines. The better the vacuum, the higher the degree of ionization of the plasma. (For this reason sometimes the paradoxical name "vacuum arc" is used.) Figure 1 shows a schematic of the hollow cathode arc used in this investigation. The gas flow through the cathode (diameter generally 13 mm) amounts to some cm^3 NTP/s. After h.f. ignition of the arc a voltage of about 100 V is sustained between the cathode and the anode in the presence of an axial magnetic field of some kGauss; the arc currents amount to some 100 A. The gas which is regenerated by recombination of the plasma at the anode and at the wall is pumped away by two 8000 l/s oil diffusion pumps at pressures of 10^{-3} Torr or less.

An extensive description of the apparatus may be found in various annual reports [1]. Its design was largely inspired by a similar device developed about twenty years ago in ORNL see [2] and [3]. Main additions are movable electrode supports and devision of the vacuum chamber in six separate sections electrically isolated from each other.

The plasma is mainly generated in a region inside and in front of the hollow cathode in a way which has some resemblences with the generation of the plasma in a glow discharge [4], but the process is as yet not understood in detail [5]. Our interest was concentrated on the plasma of the positive column (also called "external plasma") which serves as a conducting path from the cathode to the anode. All the plasma parameters in this column were measu-

---

* This work was performed under the terms of the agreement between the Technische Hogeschool Eindhoven and the association EURATOM, to conduct joint research in the field of plasma physics.

** Eingang der 1. Fassung am 18. 10. 1978.

Reprint requests to Dr. F. Boeschoten, Institut für Plasmaphysik der Kernforschungsanlage Jülich GmbH, D-5170 Jülich.

0340-4811 / 79 / 0800-1009 $ 01.00/0

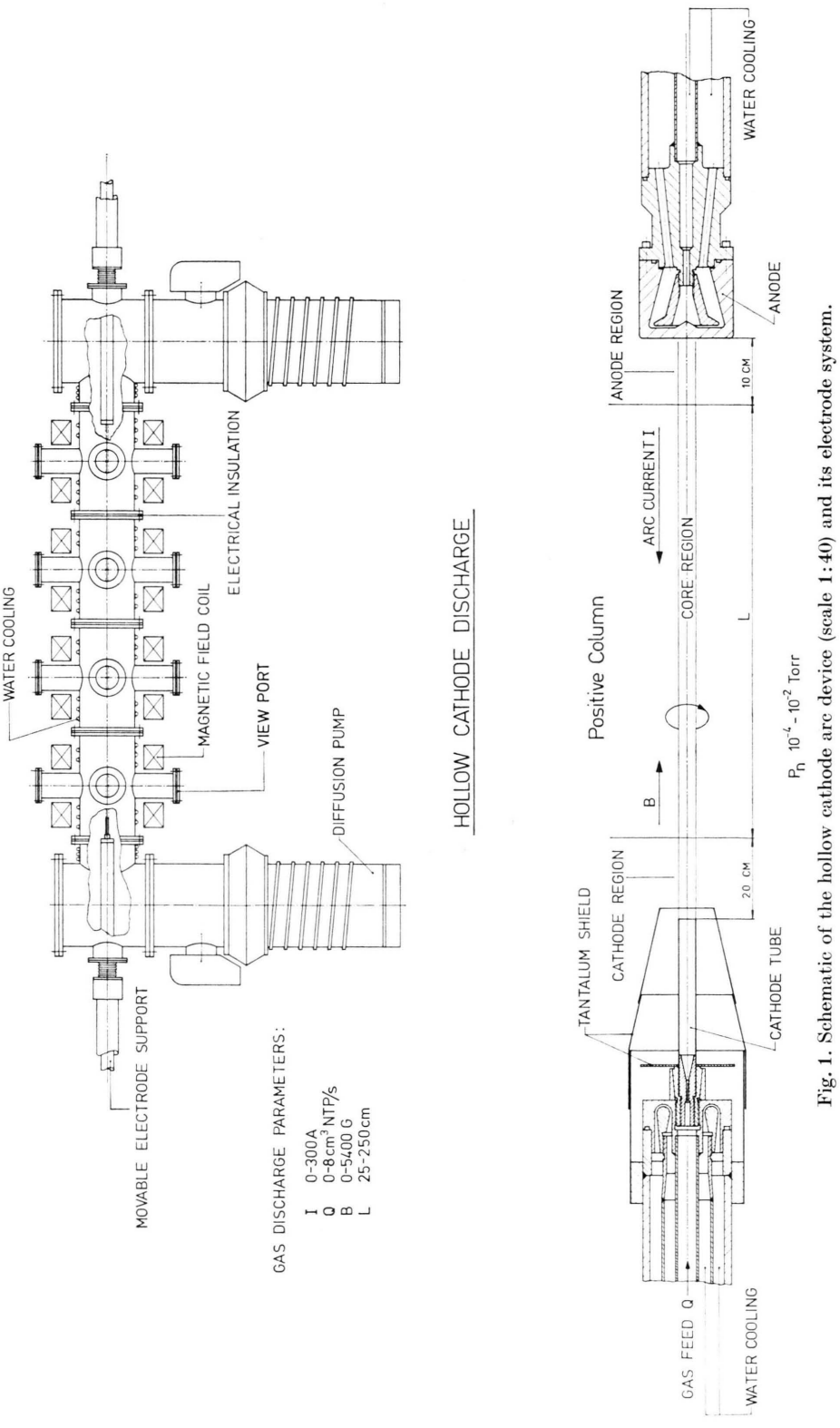

Fig. 1. Schematic of the hollow cathode arc device (scale 1:40) and its electrode system.

red as function of radial and axial position and the relations which exist between the plasma parameters according to the two fluid model [6] may be checked directly. Such a study is made in Part II of this investigation.

The degree of ionization is very high; the plasma density in the centre of this arc ($n_e \cong 10^{14}$ part./cm^3) is almost a hundred times larger than the neutral particle density, so the mean free path length for Coulomb collisions between the charged particles ($\lambda \cong 1$ cm) is two orders of magnitude smaller than for collisions with neutral particles. Depending on the magnetic field strength and on the gas which is used the cyclotron radii of the ions, r_{ci}, are in a large part of the plasma smaller than the m.f.p. length for collisions, so the plasma may be considered as a fully ionized and — magnetized plasma ($\omega_{ci}\tau_i = \lambda/r_{ci} > 1$). In these respects the plasma of the hollow cathode arc differs from the plasma in medium pressure arcs where the plasma density is much higher ($n_e \cong 10^{16}$ part./cm^3) and about equal to (or smaller than) the neutral density. The medium pressure arcs are also much smaller with the advantage of lower cost but the disadvantage of much less accessibility for diagnostics. Otherwise there are some resemblences between the two kinds of arcs, particularly in regard to temperature and mass velocity [7]. Recently detailed investigations were made to see whether the plasma rotation in these arcs may be used for isotope separation [8].

The discharge is operated continuously and runs stably for hours. The length of its plasma column may easily be varied and is always long compared to the mean free path length for the collision of an ion or electron with another particle. Due to its high temperature, the ions in this plasma emit strong spectral lines. This opens the possibility to use one of the most reliable diagnostic tools in plasma physics: Doppler broadening and -shift of spectral lines in order to measure the temperature and the directed velocity of the ions. Also the plasma density is high enough to apply another powerful diagnostic tool — Thomson scattering of laser light which was used to measure the temperature and the density of the electrons.

The plasma of the hollow cathode discharge is practically cylindrical and is in a stationary state. The attention was not only directed towards the d.c. values of the plasma parameters, but also towards the low frequency oscillations ($\nu =$ 10—20 kHz) which are generated spontaneously in the plasma. In most experiments an argon plasma was chosen because of the relatively large radii of the argon ions and the correspondingly broad density profiles; an extra advantage of argon is easy operation and low wear of the electrodes. The plasma density $n_e(r, z)$, the ion temperature $T_i(r, z)$, the electron temperature $T_e(r, z)$, the mass velocity $\mathbf{v}(r, z)$ and the plasma potential $\Phi(r, z)$ were measured with various diagnostic tools. Also some efforts were made to obtain information on the neutral density $n_n(r, z)$ and temperature $T_n(r, z)$.

The variable discharge parameters are arc current I (10—300 A), gas feed Q (0.2—8 cm^3 NTP/s), magnetic field strength B (200—5400 Gauss) and arc length L (25—250 cm). The magnetic field strength has only a component in axial direction and is practically homogeneous ($\Delta B/B < 3\%$). The induced magnetic field is small and the magnetic field strength may be considered as an independent external parameter. The length of the plasma column may be varied continuously and the core diameter was varied by using cathode tubes of various diameter, d. (For optimal operation the length of the cathode tube is taken 6 to 7 times d.)

A given set of discharge parameters corresponds to a certain set of plasma parameters. By varying one of the discharge parameters generally all plasma parameters are changed and a new equilibrium situation is created. The simultaneous changing of the plasma parameters requires great caution with the interpretation of the findings. In the following sections the phenomenal relations between the plasma- and the discharge parameters are described. ("Standard conditions" are: $L = 120$ cm, $d = 13$ mm, $B = 3400$ Gauss. $I = 100$ A and $Q = 4.5$ cm^3 NTP/s.)

The centre of the arc was taken as $r = 0$, and the electrode supports were adjusted in such a way that the axis of the arc coincided as much as possible (some mm) with the axis of the vacuum vessel. Visual observation of the arc indicates that the positive column is formed at a distance of about 20 cm from the tip of the hollow cathode tube. (This is confirmed by other observations — see e.g. Section 2.2.) This axial position was taken as $z = 0$. L is defined as the length of the positive column. Most measurements were made at the positions $(r, z) = (0, 0)$ and $(0, 50)$.

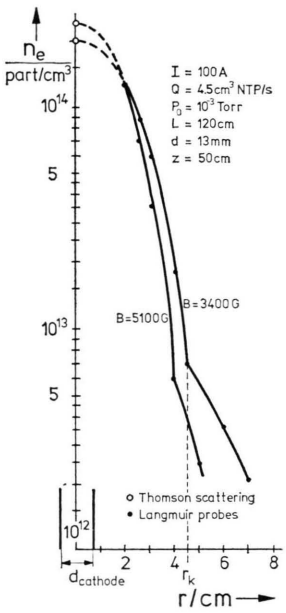

Fig. 2. Radial density profile at the middle of the positive column of a hollow cathode discharge fed with argon (standard conditions; $z = 50$ cm).

It is necessary to make a distinction between plasmas which are present in different regions of the discharge where different physical processes dominate. On the basis of the radial density profiles (Fig. 2) in radial direction a distinction is made between the core region ($0 \leqq r < d/2$), the regular plasma region ($d/2 \leqq r < r_k$) and the outside region ($r \geqq r_k$). In the core region the plasma carries an appreciable current and the radial derivative of the density may be small (depending on d). In the regular plasma region the plasma behaves as expected from the usual two-fluid model, whereas at radii larger than r_k (4 to 5 cm from the axis) the plasma is only weakly ionized and possibly turbulent. In axial direction we disregard the regions inside and directly in front of the cathode ($\Delta z < 20$ cm) and the anode ($\Delta z \simeq 5$ cm) where big voltage drops occur and where respectively ionization- and recombination processes are of particular importance. These regions are of course very essential for the existence of the plasma but are not the object of this study. We concentrate our attention to the positive column, which is most suited for studies in plasma physics.

2. The Ion Temperature

T_i was determined from Doppler width measurements of the AII 4806 Å* line, using a pressure scanned Fabry-perot interferometer with 1 mm spacing and resolving power $\lambda/\Delta\lambda > 2.5 \times 10^5$. The Stark effect is negligible and interference by the Zeeman effect is suppressed by the use of a polarisation filter. The line profiles are generally found to be approximately Gaussian (except in the tail). Thus the thermal velocity velocity distribution of the ions is in first approximation Maxwellian, though the presence of small groups of ions with different temperatures cannot be excluded.

* Other AII lines yield the same results and may be used as well.

2.1. Radial Dependence, $T_i(r)$

For all values of z and for all operating conditions it was found that within the accuracy of the measurements *the ion temperature is constant over the radius*:

$$\partial T_i / \partial r = 0 \,. \tag{1}$$

Up to $r = 4$ cm the statistical error is about 5%. At $r = 7$ cm where the intensity of the spectral line is three orders of magnitude less than at the centre, the statistical error is increased to 15%.

2.2. Axial Dependence, $T_i(z)$

Figure 3 shows the dependence of the ion temperature on the axial position in an arc of 140 cm length (standard conditions). In agreement with the visual observation it seems that the cathode region extends about 20 cm in axial direction where it changes rather abruptly into the positive column

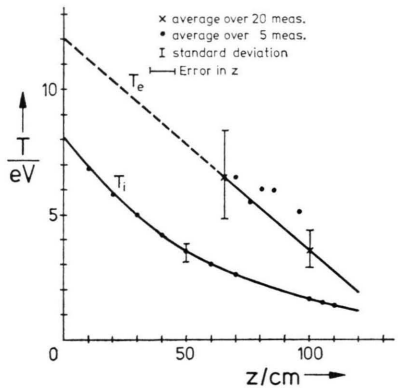

Fig. 3. Axial variation of electron- and ion temperature (standard conditions; $r = 0$ cm). T_e measurements at lower values of z were impeded by the fact that the amount of scattered light in each wave length "channel" becomes smaller by further broadening of the Doppler profile ($\Delta\lambda \sim T_e^{3/2}$) and finally drowns in the background fluctuations.

which begins at $z=0$. For varions values of Q, T_i varies approximately exponentially with z with an e-folding length, λ, of about 60 cm.

$$T_i(0,z) \cong T_i(0,0)\, e^{-z/\lambda}. \tag{2}$$

Apparently λ does not depend much on Q.

The decrease of T_i with distance from the cathode may be explained by the fact that the ions move from the cathode towards the anode (Section 6.1.) and suffer during this transit charge exchange collisions with cold neutral particles which flow from the wall towards the core of the arc.

2.3. Dependence on Current Density, $T_i(j)$

For each cathode a linear dependence of the ion temperature on the arc current, I, is found. Experiments with cathode tubes of various diameter showed that T_i *depends linearly on arc current density* $j = 4I/(\pi d^2)$.

$$T_i = \text{const}\, j \quad (\text{for } 3\text{ cm} > d > 1\text{ cm} \text{ and } j > 40\text{ A/cm}^2). \tag{3}$$

Under "standard"-conditions and at $z=50$ cm the constant $\cong 4.8 \times 10^{-2}$ eV cm^2/A.

For cathodes with diameter $d<1$ cm, the constant seems to be somewhat smaller: it might be better to use $(d+r_{ci})$ instead of d for calculation of j. The constant depends also somewhat on the thickness of the cathode tube.

2.4. Dependence on Gas Feed, $T_i(Q)$

T_i shows little variation with Q for values of Q above 4 to 5 cm^3 NTP/s. For this reason a gas inlet $Q=4.5$ cm^3 NTP/s was chosen as "standard"-condition. Below $Q=2$ cm^3 NTP/s T_i increases rapidly with decreasing Q [1]. At minimal Q and maximal I, ion temperatures up to 35 eV may be reached near the cathode.

Similar $T_i(Q)$ curves were found for various cathode diameters. If $Q/(\pi/4)\, d^2$ is used as parameter all curves coincidence within the error limits. This indicates that *the ion temperature, T_i, is a function of the gas flux* $(n\, v_z)_{gas} = 4Q/(\pi d^2)$.

2.5. Dependence on Magnetic Field Strength, $T_i(B)$

The variation of $T_i(0, 50)$ with B is shown in Fig. 4 for two values of gas feed Q (1 cm^3 NTP/s and 4.5 cm^3 NTP/s). For $Q=1$ cm^3 NTP/s the ion temperature is about one and a half time the value found for $Q=4.5$ cm^3 NTP/s, but the shape of the

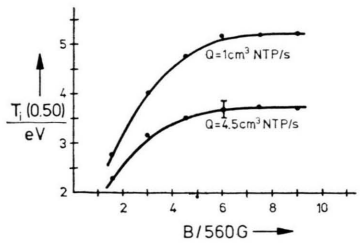

Fig. 4. Variation of ion temperature with magnetic field strength B ($r = 0$ cm; $z = 50$ cm).

curves is the same. At lower B values up to $B \cong$ 3400 Gauss the temperature increases with B, at higher B values T_i is approximately independent of B. For this reason a magnetic field strength of $B=3400$ Gauss was chosen as "standard"- condition.

The heating mechanism of the ions is unknown. Apparently the heating takes place in the cathode region and it is of interest to know how it is affected by the ratio d/r_{ci}. The ion temperatures of the plasma columns generated with cathode tubes of various diameter (fed with the same gas flux and with the same current density) all depend in the same way on B. Apparently T_i *is independent of the ratio* d/r_{ci}.

2.6. Length Dependence, $T_i(L)$

For arcs longer than 1 m $T_i(0, 0)$ increases approximately linearly with arc length L with a slope depending on Q [1]:

$$T_i(0,0) = \text{const}\, L \quad (L > 100\text{ cm}); \quad \text{const}\,(Q = 4.5) \cong 6\text{ eV/m}. \tag{4}$$

This is similar to the findings of McNally and Skidmore [9] with a carbon vacuum arc and seems to be an intriguing aspect of low pressure arcs.

3. The Electron Temperature

Only in the core of the arc the electron density is high enough ($n_e \cong 10^{14}$ part/cm^3) for yielding a detectable intensity of (Thomson) scattered light using a 30 J Ruby laser. Its detection was limited by the presence of some argon spectral lines in the vicinity of the laser line ($\lambda = 6943$ Å) and by the spontaneous fluctuations in the light emitted by the arc. (No efforts were made to overcome this latter drawback by using differential methods.)

Thus the T_e measurements in the core were limited to values below 10 eV where the scattered

radiation is distributed over a relatively small wave length range, but is of sufficient intensity to be detected above the background radiation.

At radii $r > 2$ cm T_e may be measured with Langmuir probes, possibly with relatively large systematic errors due to the presence of a magnetic field.

3.1. Radial Dependence, $T_e(r)$

Figure 5 shows that T_e drops sharply in the region next to the core — in contrast to T_i which is constant with radius. At radii $r \gtrsim 2.5$ cm: $1\text{ eV} < T_e < 2\text{ eV}$ and T_e does not vary much with radius.

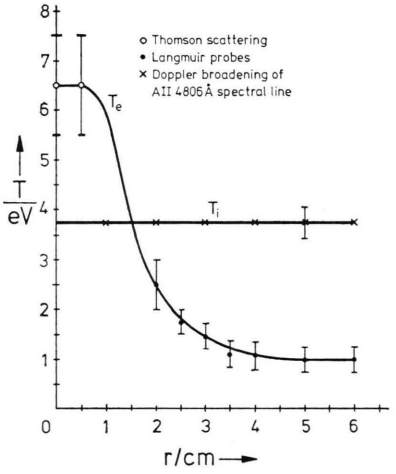

Fig. 5. Radial profile of electron- and of ion temperature (standard conditions; $z = 50$ cm).

3.2. Axial Dependence, $T_e(z)$

The electron temperature at the axis, $T_e(0, z)$, decreases from the cathode towards the anode — like T_i (Figure 3). Similar measurements made before by Gerry and Rose [10] yielded $T_e = 4$ to 6 eV. The hollow cathode discharge they used was, however, operated at much lower values of B, I and d and the data cannot be compared directly. Not much variation of T_e with z is found at radii $r > 2$ cm.

4. The Plasma Density

The probe characteristics of small Langmuir probes (1 mm diameter, 1 mm long) show a well saturated ion current and also saturation of the electron current. The radial density profile in the regular plasma region may be measured well with these probes, and in this case the absolute values of the density turned out to be less than 25% in (systematic) error. The core region is not accessible for Langmuir probes, but here Thomson scattering of laser light may be used $n_e(0) \lesssim 2 \times 10^{14}$ part/cm^3; $1\text{ eV} < T_e < 10\text{ eV}$. Fluctuations in the plasma density are responsible for a relatively high inaccuracy in the Thomson scattering experiments.

4.1. Radial Dependence, $n_e(r)$

Figure 2 shows the combined results of the probe and the scattering measurements for two values of B. In the regular plasma region the density profiles are approximately Gaussian-shaped

$$n_e(r) \cong n_e(0)^{-r^2/q^2} \tag{5}$$

with q depending on the magnetic field strength, B, and gas feed Q. For B values above about 3000 Gauss q^2 seems to vary inversely proportional to B (e.g. at $z = 50$ cm $q^2 \cong 6.4$ cm^2 at $B = 3400$ Gauss and $q^2 \cong 4.2$ cm^2 at $B = 5100$ Gauss). $n_e(0) \cong 2 \times 10^{14}$ part/cm^3 also depending on B and Q.

Under some conditions small dents in the — overall — Gaussian profiles are found. These deviations from the Gaussian profiles are possibly related to the low frequency oscillations which are generated spontaneously in the plasma (see Section 8).

The radial density profiles measured at $z = 5, 20, 35, \ldots, 115, 130$ cm all have the same shape, but apparently q^2 increases somewhat towards the anode. (Under standard conditions $q^2 \cong 8.5$ cm^2 at $z = 100$ cm.)

4.2. Axial Dependence, $n_e(z)$

The plasma density varied only weakly along the axis:

$$\frac{L}{n_e}\left|\frac{\partial n_e}{\partial z}\right| \lesssim 1.0\,. \tag{6}$$

4.3. Dependence on Fas Feed, $n_e(Q)$

Both Langmuir probe- and Thomson scattering measurements show unambiguously that *the plasma density increases with Q*. For $Q < 2$ cm^3 NTP/s (and "standard" conditions) $n_e(0)$ of Eq. (5) increases approximately linearly with Q, and q^2 also increases. For $Q > 2$ cm^3 NTP/s $n_e(0)$ does not increase much with Q any more and neither does q^2.

4.4. Dependence on Magnetic Field Strength, $n_e(B)$

As was already mentioned in Sect. 4.1 for values of $B > 3000$ Gauss:

$$q^2 = \text{const } B^{-1} \tag{7}$$

with the constant equal to 2.15×10^4 Gauss cm^2.

The improved radial confinement with B leads also to somewhat higher values of $n_e(0)$ as may be seen from Figure 2.

4.5. Dependence on Arc Current I, on Arc Length, L, and Cathode Diameter, d

Both Langmuir probe- and Thomson scattering measurements indicate that n_e increases only weakly with I. The plasma density does not depend much on L either.

For cathode diameters $d < 1$ cm, n_e increases with d; for $d > 1$ cm n_e does not vary much with d (current density and gas flux being the same).

5. The Electric Field

The I-V characteristic of the argon arc under "standard"-conditions is shown in Figure 6. Practically the only possibility to measure electric fields in the plasma is by means of Langmuir probes; due to the presence of a magnetic field and to the variation of T_e with r and z these measurements are rather problematic. Some information may also be obtained indirectly from the variation of the arc voltage with the length of the plasma column.

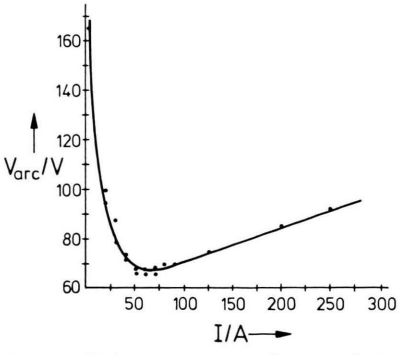

Fig. 6. Voltage-current characteristic of Argon arc. "Standard" conditions: $Q = 4.5$ cm^3 NTP/s; $B = 3400$ G; $L = 120$ cm; $d = 13$ mm.

5.1. The Voltage Distribution Along the Axis, $V(z)$

Most of the voltage drop at the cathode occurs inside the cathode region. The luminosity of the plasma in front of the cathode is lower than in the positive column. This may be related to a small "dip" in the $V(z)$ curve like occurs in the Faraday dark space of a glow discharge. The presence of such a dip is not established definitely. (For more details see [1] and [11].)

The positive column is a very good conductor: for an arc length of 1 to 2 m the voltage drop over the positive column is 10—20 V when the arc current is 100—200 A. A way of measuring E_z is described in Section 5.3.

5.2. The Voltage Distribution in Radial Direction, $V(r)$

Figure 7 shows the floating potential, V_{fl}, as function of radius for three values of B at $z = 50$ cm. The plasma potential, V_{Pl}, is determined as the potential where the "kink" in the (logarithmically drawn) electron current to the probe occurs. The plasma potential is related to the floating potential:

$$e V_{Pl} = e V_{fl} + C k T_e ,$$

where $C \cong (1/2) \ln (m_i/m_e)$ is expected to be about 5 for argon [12]. From these measurements and from Fig. 5 C is found to be about 3.

It follows from Fig. 7 that a relatively large inwardly directed radial electric field is present near the core of the arc. This field is evidently related with the rotation of the arc column. Its theoretical derivation is given in Part II of this investigation [11].

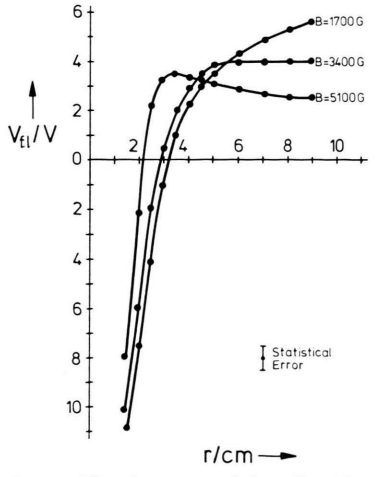

Fig. 7. Floating potential as function of radius for various values of B ($z = 50$ cm).

5.3. Variation of Arc Voltage with Arc Length, $V(L)$

For an arc length $L \gtrsim 50$ cm, the arc voltage varies linearly with L. If it is assumed that like in the glow discharge the voltage drops at the anode and at the cathode are not changed noticeably when the length of the arc is changed, the measured variation of the voltage drop over the discharge, ΔV, equals the variation of V over the positive column, and it is expected that $E_z \cong \partial V/\partial L$. (As T_e varies with L, ΔV is not only brought along by a variation in length, but also by a variation of the conductivity; this effect is, however, for the larger part compensated by the simultaneous variation of the electron pressure.)

The electrical conductivity at $z=0$ is found to be $\sigma_0 \cong 1000\ \Omega^{-1}\ \mathrm{cm}^{-1}$, which is in good agreement with its theoretical value $\sigma_0 \cong 20\ T_e^{3/2}[\mathrm{eV}]$ and seems to be a strong indication that the electrical conductivity in the core region is normal. This conclusion is confirmed by the calculations in Part II of this investigation [11].

6. The Mass Velocity

Temperature control and optimal adjustment of the (1 mm) étalon Fabry Perot spectrometer makes it possible to measure directional velocities by Doppler shift with a limit of detection of about 1.5×10^4 cm/s ($\Delta\lambda \cong 2.5$ mÅ). In the region 2 cm $\leqq r \leqq 6$ cm the mass velocity may also be measured with a pendulum [13] and with directional Langmuir probes [14] and [15].

6.1. The Axial Velocity, v_z

Head on Doppler shift measurements revealed that in the core region the plasma moves from the cathode towards the anode with a velocity $v_z \cong 6 \times 10^4$ cm/s (see also [16]). The same values were also found with the pendulum at various radial ($r=2$ cm and $r=3$ cm) and axial ($z=0$ and $z=60$ cm) positions. It is concluded that *the plasma moves as a whole from the cathode towards the anode with a velocity*

$$v_z = (6 \pm 3) \times 10^4\ \mathrm{cm/s}\,. \tag{9}$$

6.2. Radial Dependence, $\Omega(r)$

The Doppler shift measurements of the azimuthal velocity $v_\theta = \Omega r$ are complicated by the fact that the optical system receives an integrated amount of light of a plasma slab with varying values of n_e and Ω. Thus a deconvolution, or inversion procedure has to be applied to the measured profiles. A digital treatment of the interferometric data [1] shows that Ω values found with and without inversion differ only 10% (about twice the statistical experimental error).

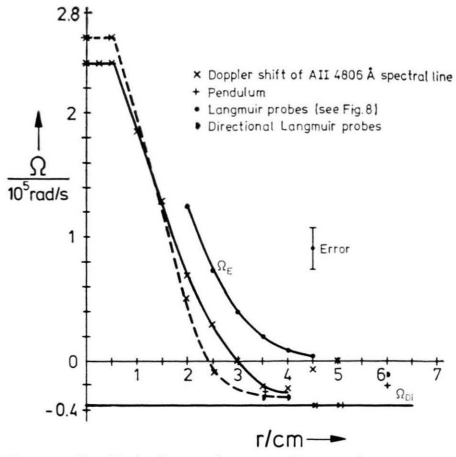

Fig. 8. Radial dependence of angular mass velocity, Ω, at $z = 50$ cm (——— standard conditions and – – – $B =$ 5100 G). $\Omega_{Di} = -2\,ckT_i/eBq^2$ is the angular frequency associated with the ion diamagnetic current. $\Omega_E = -(c/r)(E_r/B)$ is derived from Fig. 7 (E_r is negative). $\Omega = \Omega_E + \Omega_{Di} - \Omega^2/\omega_{ci}$.

The $\Omega(r)$ curves measured at $z=50$ cm under "standard"-conditions, and for $B=5100$ Gauss are shown in Figure 8. In the core region the angular mass velocity, $\Omega(0, 50)$, is constant and in the direction of the diamagnetic electron current (positive direction). In the regular plasma region Ω is strongly sheared and even changes sign at $r \cong 3$ cm. The direction of rotation reverses, if the magnetic field is directed oppositely.

The angular electrical field drift $\Omega_E = -(c/r)(E_r/B)$ (derived from Fig. 7) is also depicted in Fig. 8, together with the angular diamagnetic drift velocity $\Omega_{Di} = -2ckT_i/eBq^2$ (derived from Fig. 2 and $T_i(0, 50) = 3.6$ eV). It may be seen that within the error limits

$$\Omega = \Omega_E + \Omega_{Di} - \Omega^2/\omega_{ci}\,. \tag{10}$$

For $r<2$ cm the electrical field cannot be measured and the centrifugal drift (Ω^2/ω_{ci}) gives an appreciable contribution to Ω.

6.3. Axial Dependence, $\Omega(z)$

For all values of z the $\Omega(r)$ curves are of the same shape, but the absolute value of Ω decreases with z. Figure 9 shows $\Omega(0, z)$ as function of z for two

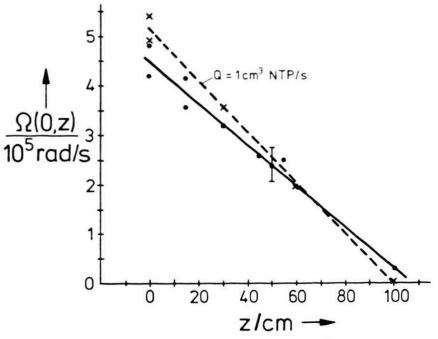

Fig. 9. Axial variation of angular mass velocity at the centre of the plasma column (——— standard conditions; – – – $Q = 1$ cm³ NTP/s).

values of the gas feed ($Q = 4.5$ cm³ NTP/s and $Q = 1$ cm³ NTP/s). Apparently $\Omega(0, z)$ decreases linearly with z.

6.4. *Dependence on Magnetic Field Strength, $\Omega(B)$*

Figure 10 shows the variation of $\Omega(0, 50)$ with B for two values of Q. The shape of the curves resembles the shape of the $T_i(B)$ curves, which indicates that $\Omega(0, z)$ and T_i depend approximately in the same way on B.

The dependence of the radial Ω profiles on B may be seen in Figure 8.

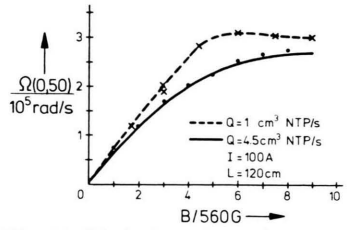

Fig. 10. Variation of angular mass velocity with magnetic field strength B ($r = 0$ cm, $z = 50$ cm).

6.5. *Dependence on Gas Feed, $\Omega(Q)$, and on Discharge Current, $\Omega(I)$*

$\Omega_0(0, 50)$ is found to increase with decreasing values of Q when $Q < 2$ cm³ NTP/s, but not as rapidly as $T_i(0, 50)$.

Ω(axis) increases linearly with I like T_i and their relation is given approximately by:

$$\Omega(0, 50) \simeq 0.5\, T_i(0, 50)\,[\mathrm{eV}] \times 10^5 \text{ rad/s}\,. \quad (11)$$

6.6. *Dependence on Discharge Length, $\Omega(L)$, and on Cathode Diameter, $\Omega(d)$*

Ω varies linearly with L and Eq. (11) holds also for various values of L.

Comparing cathodes of various diameters seems to be most meaningful if gas flux and current density are the same. Under this condition the $T_i(B)$ and $\Omega_0(B)$ curves for cathodes of various diameters roughly coincide.

6.7. *The Radial Velocity, v_r*

In the direction of the anode the core appears more diffuse: its radius increases and its luminosity decreases. Under "standard"-conditions $\Delta r \lesssim 2$ mm per m arc length. (Δr decreases with increasing B.) This yields at the edge of the core an upper limit $v_r \lesssim 2 \times 10^{-3}\, v_z \simeq 120$ cm/s.

7. The Neutral Particles

The gas discharge results as an interplay between the applied voltage and the gas. The created plasma does not only depend strongly on the amount of gas which is fed to the discharge, but also on the way the gas feed (and pumping) takes place. Besides on the gas flow the distribution of the neutrals depends on the interaction of the plasma with the neutral gas, like ionization (mainly in the active zone), recombination (mainly at the wall and at the anode) and charge exchange (pumping action of the discharge). The positive column is the simplest part of the arc; it serves as a conduting path for electricity and heat.

Information about the distribution of the neutral particles was obtained from pressure measurements with ionization gauges and from the intensity of spectral lines. The temperature, T_n, and the velocity, v_n, of the neutrals were derived from Doppler broadening and -shift of the AI 4201 Å line measured with the interferometer.

7.1. *The Neutral Density, n_n*

From the spectroscopical observations the neutral particle density in the core region is estimated to be $n_n(0) \simeq 10^{12}$ part/cm³. At the wall (where $T_n = 20$ °C) the neutral gas pressure is about 7×10^{-4} Torr and so there $n_n(R) \simeq 2 \times 10^{13}$ part/cm³. It also raises considerably in the neighbourhood of the anode, where a large part of the plasma particles recombine [17]. Some indication about the value of n_n at intermediate radii was obtained by introducing a tantalum tube ($\varnothing =$ 6 mm) into the plasma and by measuring the pressure at the other and of this tube, p_n, as function

of the radial position of the snout. It was found that outside the core $n_n(r)$ increases rapidly [1]. *The arc clearly works as a pump.*

7.2. The Temperature of the Neutrals, T_n

The temperature of the neutral particles on the axis, $T_n(0, z)$ seems to be approximately equal to the ion temperature $T_i(0, z)$. Apparently the Doppler width of the neutral AI lines emitted from the core region is determined for a large part by neutral particles which originate from charge exchange or recombination. The presence of a big groups of cold neutrals cannot be excluded. Outside the core region the temperature of the neutral particles drops rapidly.

7.3. The Angular Velocity of the Neutrals, Ω_n

Accordingly the angular velocity of the neutral particles in the core region was found to be not much less than the angular velocity of the ions. Within the accuracy of the measurements (about 20%): $\Omega_n(0, z) \lesssim \Omega_i(0, z)$.

7.4. Operation of the Arc with Gas Feed Through the Anode

When the gas is fed through the anode, the values of Ω_0 and T_i at $z = 50$ cm are practically the same as when the gas is fed through the cathode. But more towards the cathode (smaller values of z) Ω_0 and T_i are lower than by feeding gas through cathode. The arc column is more homogeneous and accordingly the contours of the core boundary are sharper. It seems worthwhile to make a closer investigation of this way of operation, which was used before by Gibbons and Mackin [3].

8. The Low Frequency Oscillations

Low frequency oscillations ($\omega \ll \omega_{ci}$) are found in the floating potential and in both the ion- and electron saturation currents of Langmuir probes, all with the same frequency. The spectrum of the probe signals is usually analysed by calculating power spectral density functions from correlation functions. Using two probes located at different positions in the arc the propagation of the waves can be measured from the phase shift in the frequency peaks in the cross-power spectral density function of the two singals. For a detailed description of these measurements see [1].

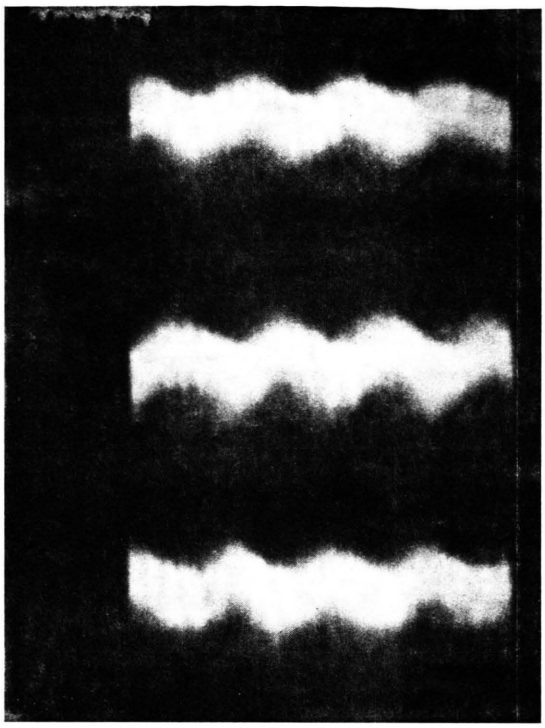

Fig. 11. Streak photograph of the core of the arc (streak length 200 μs; slit width 0.5 mm; $z = 60$ cm).

The peaks in the power spectral density function of the fluctuations in the intensity of the spectral lines emitted by the plasma correspond exactly to those of the Langmuir probe signals.

Streak pictures of a narrow slit perpendicular to the plasma column show also large amplitude oscillations of the arc with the same frequency (Figure 11).

Combining the results of the measurements leads to the conclusion that *the whole arc including the core region is oscillating with the same frequency. The oscillations are due to a $m = 1$ mode* which propagates in the same direction and with about half the velocity of the mass rotation in the centre of the arc.

8.1. Frequency of the Oscillations

Measurements of the oscillation frequencies have been made under a large variety of operating conditions. *The frequency of the oscillations was found to be independent of axial and radial position.* A number of characteristic results is presented in this section. In most measurements the power spectral density function contained only one

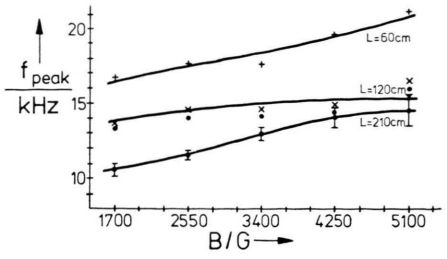

Fig. 12. Frequency of the l. f. oscillations as function of magnetic field strength B. ● Theoretical values of the frequency for an arc of 120 cm length [20].

discrete frequency peak; in a few cases also higher harmonics were found.

Figure 12 shows the oscillation frequency as a function of B for different arc lengths. The measurements show a rather weak dependence of the oscillation frequency on the magnetic field strength. For decreasing values of Q the frequency rises very rapidly as was also found to be the case with $\Omega(0)$.

8.2. Amplitude of the Oscillations

The amplitude of the oscillations turned out to be strongly radial dependent. Figure 13a shows the amplitude of the floating potential oscillation as a function of radius. The a.c. part of the ion and electron saturation on currents varies similarly with r (Figure 13b).

From Fig. 13a the azimuthal a.c. electric field near the core is found to be $\tilde{E}_\varphi \cong 2$ V/cm. This $\tilde{E}_\varphi$ field causes a perpendicular a.c. drift of the plasma particles with velocity $\tilde{v}_d \cong 6 \times 10^4$ cm/s. As the angular frequency of the oscillations $\omega \cong 10^5$ rad/s the particles move around their equilibrium position over a distance $\Delta r = \tilde{v}_d/\omega \cong 0.6$ cm. This estimate, based on the results of the probe measurements, agrees well with the direct observation made with the streak camera (Figure 11).

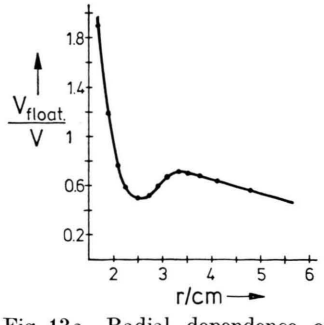

Fig. 13a. Radial dependence of the amplitude of the l. f. oscillations in the floating potential.

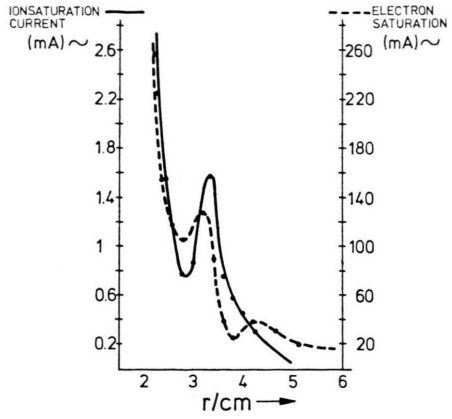

Fig. 13b. Radial dependence of the amplitude of the l. f. oscillation in the ion saturation current (———) and in the electron saturation current (– – –) to a Langmuir probe.

8.3. Phase Measurements

Measurements with two probes at the same radial and azimuthal but at different axial positions (distance between the probes 66 cm) show *no axial phase-shift in the oscillation of the floating potential.*

Figure 14 shows the radial dependence of the phase in the oscillation of the floating potential, when two probes are placed under an azimuthal angle of 90° relative to the centre of the arc at the same axial position with one probe at a fixed radial position, while the radial position of the other probe is varied. When the probes are at the same radius $r = 3.3$ cm, the phase difference is 90°. From these measurements (together from the fact that oscillations picked up by diametrically opposed probes are 180° out of phase) it was concluded that *an $m = 1$ wave propagates azimuthally in the direction of an electron in its gyro circle. Furthermore there is a phase-lag between points at smaller radii relative to points at larger radii.*

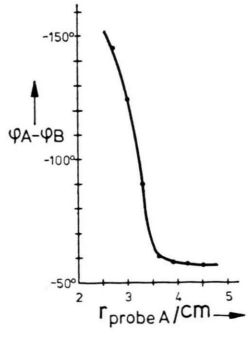

Fig. 14. Radial dependence of the phase shift in the l. f. oscillation with probe P_B in a fixed position at $r = 3.3$ cm.

8.4. Identification of the Oscillations

Identification of the wave is complicated by the fact that the amplitude of the oscillations is so large that we are certainly dealing with a non linear phenomenon and furthermore by the non uniformity of the plasma. As the frequency of the oscillations does not depend on z, whereas the plasma parameters T_i, T_e and Ω vary considerably along the axis, the mode represents apparently an average property of the plasma.

The characteristics of the oscillations are precisely those of *the transverse Kelvin-Helmholtz instability* which has its origin in the strong shear in the plasma rotation. Identification of the stability was facilitated considerably by a very detailed study of Jassby [18]. In this study a comparison is made with other instabilities which would give rise to oscillations of about the same frequency (centrifugal and resistive drift). At the hand of Table 1 and Fig. 3 and of the eight point criteria list of that article the reader may convince himself that we have univoquely to do with the Kelvin-Helmholtz instability. The important parameters there

$$\Omega_E(\max)/\Omega_{Di} \quad \text{and}$$
$$S/\Omega_E(\max) = (L_\perp/L_\parallel)^2(\omega_{ce}\,\tau_e)(\omega_{ci}/\Omega_E(\max))$$

are found from Fig. 9 to be respectively 9 and 0.1 in our case; $\tilde{n}/n \cong 0.1$ (Fig. 13b) and $e\varphi/kT_e \cong 0.5$ (Figure 13a). Another study of these oscillations was made by Rognlien [19].

Recently Janssen gave a quantitative description of the waves on the basis of a non ideal MDH theory which gives proper account of the fact that $\Omega_E(\max)$ is much larger than Ω_{Di} [20]. The results of his numerical calculations are shown in Figure 13.

9. Radiation Measurements

The radiation from the plasma was measured with a thermopile and with a HP 5082—4220 pin photo diode (sensitive to radiation in the range of 4000 to 10000 Å). Under standard conditions the total radiation power emitted from the argon arc was found to be about 40 Watt, of which about a quarter in the visible range. The recombination time in the core region is estimated to be $\tau_{rec} \cong 10^{-3}$ s. Thus about $1.6 \times 10^{-19}\,(n_e/\tau_{rec})(\pi/4d^2 L\chi_i) \cong 35$ Watt is expected to excape from the positive column by radiative recombination, in agreement with the measurements (χ_i is ionization potential). This is only about 1% of the total power which is handled by the positive column.

10. Various Gases

Besides varying n_e, T_i, T_e, **B**, **v** and **E**, it seems also of interest to vary the ion mass m_i. For that purpose the arc was run with various other gases: H_2, He, N_2 and Ne. The values of the plasma parameters are determined by the atomic processes suffered by the neutral particles, like ionization, recombination and charge exchange which differ for the various gases. For every gas the plasma finds its own equilibrium situation which may differ considerably from the situation in the argon arc.

10.1. D.C. Properties

Table 1 shows some plasma data which were measured in arcs fed with various gases under standard conditions. The plasma density, n_e, and the electron temperature, T_e, are absent in this table as it turned out to be impossible to make with the present 30 J ruby laser Thomson scattering measurements in other gases than argon and helium. All arcs are started with argon gas. The desired gas is fed additionally to the arc, whereupon the argon feed is stopped. In the table are also shown the maximum ionization cross sections for

Table 1. N. C. values of arc fed with various gases.

Gas	χ_i	$\sigma_{i\max}$	E_{opt}	Color arc	V_{arc}	$T_i(0,0)$	$T_i(0,50)$	$\Omega(0,0)$	$\Omega(0,50)$
A	15.75	3.1	70	blue	70	9 ±1	3.6±0.3	4.5±0.5	2.5±0.3
N_2	14.5	1.5	100	light blue	115	8 ±1	3.3±0.4	4.8±0.5	3.0±0.5
Ne	21.6	0.8	160	pink	120	7.8±1	4.0±0.4	5.0±0.5	3.0±0.5
He	24.6	0.37	120	faint-pink	210	11 ±2	8 ±2	5 ±1	3.5±1
H_2	13.6	0.65	60	faint-l. blue	180	—	—	—	—

χ_i = ionization potential in V; $\sigma_{i\max}$ = maximum ionization cross section in 10^{-16} cm^2; E_{opt} = electron energy in eV corresponding to $\sigma_{i\max}$; V_{arc} = voltage over the arc in V; T_i = ion temperature in eV; Ω rotational mass velocity at $r = 0$ in 10^5 rad/s.

the various gases and the voltages where this maximum is reached (from [21]). The voltage over the arc is clearly lower for gases with a higher cross section for ionization.

The nitrogen arc is very similar to the argon arc, only the radial gradient in the density is somewhat steeper. The neon arc resembles also the argon arc, but its operation is somewhat less stable. Apparently the ion temperature T_i, and the rotational velocity Ω are approximately the same for the various arcs.

Helium and hydrogen vacuum arcs are difficult to run because of unfavourable I—V characteristics leading to unstable operation. Though the arcs are operated with a current stabilized rectifier, the use of these gases requires an additional resistance of about 1 Ω in series with the arc. Moreover the high voltage drops in the helium and the hydrogen arcs cause a very heavy wear of the electrodes which makes operation of these arc less easy.

10.2. Low Frequency Oscillations

The frequency of the oscillations in the *nitrogen* plasma is about 1.5 times the frequency found in argon and depends in the same way on B, Q and I. In the *neon* plasma two frequencies are found and comparison is not possible at the present state of the theory. In the *helium* plasma the frequency is about three times higher than in argon.

Acknowledgements

The authors are indebted to L. H. Th. Rietjens for the support he has given to this work and for many useful discussions. They also like to acknowledge the skilful assistance of A. W. M. van Iersel and M. L. Rutten. Most of the measurements of the low frequency oscillations were made by D. J. Kleijn, and W. F. H. Merck had a great part in the Thomson scattering experiments.

[1] Euratom-THE Group, Experiments with a Large Sized Hollow Cathode Discharge Fed with Argon, T. H. Eindhoven-Reports 74-E-45 (1974), 75-E-59 (1975), and 76-E-67 (1976).
[2] J. S. Luce, Proc. 2nd U. N. Conf., Peaceful Uses Atomic Energy **31**, 305 (1958).
[3] R. A. Gibbons and R. J. Macking, Proc. 5th Int. Conf. on Ionization Phenomena in Gases **1961**, 1769.
[4] A. von Engel und M. Steenbeck, Elektrische Gasentladungen, Springer-Verlag, Berlin 1934.
[5] J. L. Delcroix and A. R. Trindade, Hollow Cathode Arcs, Advances in Electronics and Electron Physics, Vol. 35, Academic Press, New York 1974.
[6] S. I. Braginskii, Transport Processes in a Plasma, Rev. Plasma Physics **1**, Consultants Bureau, New York 1966.
[7] C. Mahn, H. Ringler, and G. Zankl, Z. Naturforsch. **23a**, 867 (1968).
[8] F. Boeschoten and N. Nathrath, in: Topics in Applied Physics, Vol.35, Uranium Enrichment, Ed. Villani, S., Springer-Verlag, Heidelberg 1979.
[9] J. R. McNally and M. R. Skidmore, Appl. Optics **2**, 699 (1963).
[10] E. T. Gerry and D. J. Rose, J. Appl. Phys. **37**, 2715 (1966).
[11] P. A. E. M. Janssen and F. Boeschoten, An Investigation of the Positive Column of a Hollow Cathode Discharge in a Magnetic Field, Part II, to be published in this journal.
[12] F. F. Chen, Electric Probes, in: Plasma Diagnostic Techniques, Academic Press, New York 1965.
[13] F. Boeschoten and L. J. Demeter, Plasma Phys. **10**, 391 (1968).
[14] F. Boeschoten and F. Schwirzke, Nucl. Fusion **2**, 54 (1962).
[15] M. Hudis and L. M. Lidsky, J. Appl. Phys. **41**, 5011 (1970).
[16] B. van der Sijde and P. A. W. Tielemans, Proc. 10th Intern. Conf. Ionized Gases, Oxford 1971, p. 192.
[17] R. Cano, M. Mattioli, and B. Zanfagna, Fontenay Rep. EUR-CEA-FC-312 (1965).
[18] D. L. Jassby, Phys. Fluids **15**, 1590 (1972).
[19] T. D. Rognlien, J. Appl. Phys. **44**, 3505 (1973).
[20] P. A. E. M. Janssen, Proc. 13th Intern. Conf. Ionized Gases, Berlin (1977).
[21] W. Lotz, Electron Impact Cross Sections and Ionization Rate Coefficients for Atoms and Ions, I.P.P. Garching-Report 1—47 (1966).